Engineering Journal issn: 0125-8281

Article

Downwash Investigation of Horizontal Tail Plane Configuration for 19-Passenger Aircraft Based on a Wind Tunnel Test

Dana Herdiana[a,*], **Sinung Tirtha Pinindriya**[b], **Arifin Rasyadi Soemaryanto**[c], **Agus Aribowo**[d], **Deasy Tresnoningrum**[e], **and Agus Suprianto**[f]

National Research and Innovation Agency (BRIN), Bogor, 16350, Indonesia
E-mail: [a,*]dana006@brin.go.id (Corresponding Author), [b]sinu002@brin.go.id, [c]arif037@brin.go.id, [d]agus076@brin.go.id, [e]deas002@brin.go.id, [f]agus137@brin.go.id

Abstract. An investigation has been conducted on wind tunnel test data of 19-passenger aircraft to see the phenomena of the downwash effect. The objective of this investigation is to analyze the downwash effect on the variation of horizontal tailplane configuration that is installed on the vertical tailplane of the aircraft and on the variation of flap configuration. Each flap configuration represents the condition at the flight profile of cruise, takeoff, and landing. The horizontal tailplane configuration is varied by changing the angle of incidence and the vertical position on the vertical tailplane. Analytic calculation was conducted on wind tunnel result data to quantify the downwash effect. A computational fluid dynamic simulation is performed to obtain the visualization of the downwash effect and for wind tunnel data verification. From the investigation, it is found that the lower position of the horizontal tail has a smaller amount of downwash than other positions. The flap configurations have greatly affected the perceived amount of downwash. The greater deflection of the flap generated downwash even more.

Keywords: Wind tunnel, flap deflection, downwash, Horizontal Tail Plane (HTP).

ENGINEERING JOURNAL Volume 28 Issue 12
Received 31 May 2024
Accepted 21 November 2024
Published 31 December 2024
Online at https://engj.org/
DOI:10.4186/ej.2024.28.12.29

DOI:10.4186/ej.2024.28.12.29

1. Introduction

In designing an aircraft, it is necessary to verify the calculation results, for example, in the downwash calculation. One tool that can be used to verify the results of aerodynamic calculations is a wind tunnel. In the case of a 19-passenger aircraft, the wind tunnel used for verification is a wind tunnel with subsonic speeds, while the type of test to be carried out is adjusted to the needs. Many things can be verified using a wind tunnel, such as the effectiveness of the control plane, the basic characteristics of the aircraft, and knowing the amount of downwash. Downwash is the flow of air forced down by the aerodynamic action of a helicopter wing or rotor as part of a process that generates lift [1] [2]. In the case of conventional aircraft, the wings are placed in front of the tail horizontally.

According to Brebner [3], there are differences in aircraft control methods, such as tail control, canard control, jet reaction control, thrust vector control, and others. Investigation of the effect of the fuselage on the amount of wing downwash flowing into the tail stream plane at low angles of attack. Brebner found that the fuselage decreases the downwash of the tail, which is known as the fuselage upwash effect [3], [4]. The downwash investigation of the tail will be carried out using the wind tunnel method, and the visualization will use the numerical method.

To find out the characteristics of an airplane, aerodynamic testing was carried out in a wind tunnel on an airplane test model [5]. The Wind Tunnel Facility named Indonesian Low-Speed Tunnel (ILST) was used to carry out the tests. This facility is part of the National Aerodynamics, Aeroelastic, and Aeroacoustic Laboratory (B2TA3), Agency for the Assessment and Application of Technology (BPPT) [6]. The general specifications of the ILST area test section are 4 x 3 m^2, the maximum wind speed is 110 m/s, and the Reynolds number obtained is 6.0E+6. Test results will be obtained, and data processing will be carried out during testing in the wind tunnel.

In processing wind tunnel data, several data must be further processed, including data processing for downwash calculations. In conventional aircraft design, wing downwash is a matter of concern because it impacts the horizontal tail characteristics. The horizontal tail provides sufficient static stability in pitch up to the rearmost center-of-gravity position [7]. Stability is very important for airplanes during flight because the nose-up tilt exacerbates the nose-up tilt in cases of instability [7].

In data processing related to this downwash, data is obtained from the results of wind tunnel testing in the form of data on the condition of the aircraft without a tail (tail off) and the condition of the aircraft with a tail (tail on), with variations in the tail angle of 0° and 5° to the x-axis (longitudinal) plane. In addition to the data processing mentioned above, data processing is also carried out with different Horizontal Tail Plane (HTP) positions; three configurations are being analyzed. In Computational Fluid Dynamics (CFD) simulation using Ansys CFX, with different HTP positions, three configurations are being analyzed.

2. Methodology

Data processing for downwash calculations is one of the many objectives of carrying out wind tunnel tests. The test was carried out in a wind tunnel by varying the tidal position of the HTP. The variation of the position that is used to process the data is taken from three data. The three data positions are given symbols, namely H61, H62, and H63 (Fig. 1). The data is processed to obtain the downwash angle caused by the wing to the horizontal tail.

Downwash on the horizontal tail affects the angle of attack (α) of the horizontal tail, so the angle of attack felt by the horizontal tail is not the same as the angle of attack of the plane.

2.1. CFD Analysis

The rate of movement of the downwash flow can be determined using the Navier-Stokes equation approach. The Shear Stress Transport (SST) model used is a combination of two turbulence models, namely the *k–ε* and the *k–ω* models [8].

The model *k–ε* relates to the eddy viscosity T, turbulent kinetic energy k, and the dissipation rate ε :

$$\mu_T = \rho C_\mu \frac{k^2}{\varepsilon} \tag{1}$$

The transport equations for the turbulent kinetic energy k and the turbulent dissipation rate ε are determined by Eq. (2) and (3), respectively [9]:

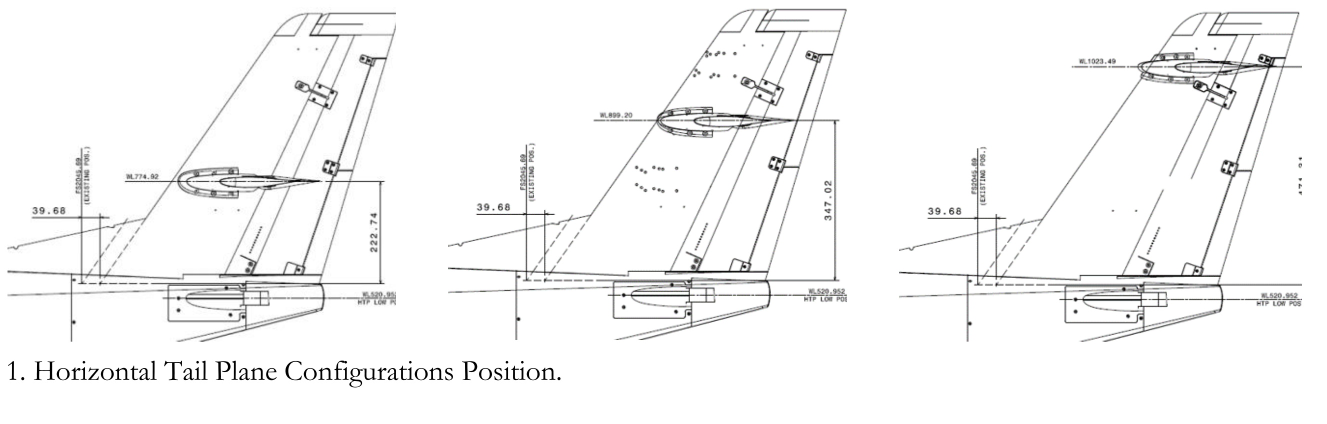

Fig. 1. Horizontal Tail Plane Configurations Position.

$$\rho\frac{\partial k}{\partial t}+\rho U_j\frac{\partial k}{\partial x_j}=\tau_{ij}\frac{\partial U_i}{\partial x_j}-\rho\varepsilon\omega+\frac{\partial}{\partial x_j}\left[\left(\mu+\frac{\mu_t}{\sigma_k}\right)\frac{\partial k}{\partial x_j}\right] \quad (2)$$

$$\rho\frac{\partial \varepsilon}{\partial t}+\rho U_j\frac{\partial \varepsilon}{\partial x_j}=C_{\varepsilon 1}\frac{\varepsilon}{k}\tau_{ij}\frac{\partial U_i}{\partial x_j}-C_{\varepsilon 2}\rho\frac{\varepsilon^2}{k}+\frac{\partial}{\partial x_j}\left[\left(\mu+\frac{\mu_t}{\sigma_\varepsilon}\right)\frac{\partial \varepsilon}{\partial x_j}\right]$$
(3)

with the following coefficient values

$$C_{\varepsilon 1}=1.44; C_{\varepsilon 2}=1.92; C_\mu=0.09; \sigma_k=1.0; \sigma_\varepsilon=1.3$$
(4)

Similar to the *k*–*ε* model, the *k*–*ω* model relates the eddy viscosity νT to the turbulent kinetic energy k but uses a different dissipation rate ω :

$$\mu_T=\rho\frac{k}{\omega} \quad (5)$$

The transport equations for the turbulent kinetic energy k and the turbulent dissipation ratio ω are defined by Eq. (6) and (7), respectively [1], [10] :

$$\rho\frac{\partial k}{\partial t}+\rho U_j\frac{\partial k}{\partial x_j}=\tau_{ij}\frac{\partial U_i}{\partial x_j}-\beta'\rho k\omega+\frac{\partial}{\partial x_j}\left[\left(\mu+\frac{\mu_t}{\sigma_k}\right)\frac{\partial k}{\partial x_j}\right]$$
(6)

$$\rho\frac{\partial \omega}{\partial t}+\rho U_j\frac{\partial \omega}{\partial x_j}=\alpha\frac{\omega}{k}\tau_{ij}\frac{\partial U_i}{\partial x_j}-\beta\rho\omega^2\omega+\frac{\partial}{\partial x_j}\left[\left(\mu+\frac{\mu_t}{\sigma_\omega}\right)\frac{\partial \omega}{\partial x_j}\right] \quad (7)$$

The *k*–*ω* model is more accurate in near-wall modeling than the *k*–*ε* model; the *k*–*ω* model has shown a perturbing sensitivity to the freestream value for ω at the boundary edge, through the inlet value [11]. The resulting basic turbulence model can combine the advantages and the equation ω [12]. One of the turbulence models, such as the Shear Stress Transport (SST) model, has gained wide users in CFD applications related to aerodynamics [13].

The Shear Stress Transport (SST) model was proposed by Menter [12] as a combination of the *k*–*ε* model and the *k*–*ω* model. The integration of the turbulence model is achieved by multiplying the transformed *k*–*ε* model and the *k*–*ω* model by factors (F1) and (1 F1). F1 is a mixed function between one and zero, depending on the distance from the wall. The value of one corresponds to the position on the wall, and the value of zero to the distance from the wall. As a result, the *k*–*ω* model is used close to the wall, in the combined boundary layer of the *k*–*ε* and *k*–*ω* models, and outside the boundary layer only the *k*–*ε* model is adopted. A general description of the implementation of the SST model in ElliSys CFD code is described by Sorensen [14]. The other research was conducted by Agus using the SST turbulence model to analyze the blockage effect for pusher propeller aerodynamic performance of lightweight UAVs compared with the experimental set-up [15].

2.2. Simulation Parameter

The condition of the simulation can be seen in Table 1. below.

Table 1. Parameter setup for simulation.

Solver	CFX
Turbulent Model	Shear Stress Transport
Spatial Discretization Scheme (Advection)	High Resolution / 2nd Order Upwind Difference
Turbulent Numeric	High Resolution
Material	Air ideal gas (air)
Density	1,159 kg/m³
Viscosity	1,48 x 10-5 kg/m-s
Operation Pressure	100400 Pa
Boundary condition Inlet	Velocity Inlet
Boundary condition of Aircraft	No Slip Wall
Boundary condition of Wind Tunnel Walls	No Slip Wall
Boundary condition Outlet	Opening
Flow velocity	70 m/s
The angle of attack (α)	-4°, 0°, 4°, 8°, 10°, 12°, 14°, 15°, and 16°

The mesh quality (Fig. 2) for this 19-passenger aircraft simulation model uses several settings, namely using the thickness of the first boundary layer (y+) at 1.09766E-05. The fineness level of the mesh density is chosen as High because it can well calculate the surface of the simulation model.

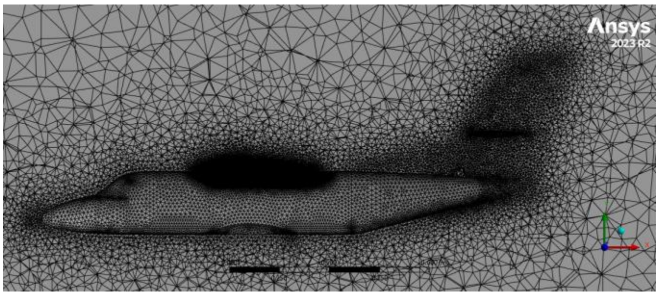

Fig. 2. Mesh Quality [16].

To know whether the simulation results can be trusted or credible, grid independence needs to be carried out. This grid independence is carried out by differentiating the number of elements. The number of elements selected is from 1 million to 51 million. The following are the grid independence results seen from aerodynamic forces and pitch moment (Fig. 3 and 4).

From the grid independence results, the number of elements that will be used in the simulation can be selected, namely around 40 million.

DOI:10.4186/ej.2024.28.12.29

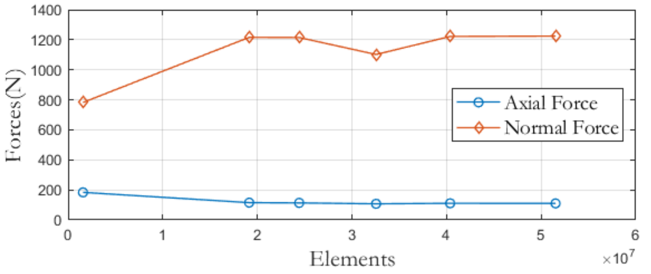

Fig. 3. Forces in axial (x-axis) and normal (y-axis) for aircraft wall body.

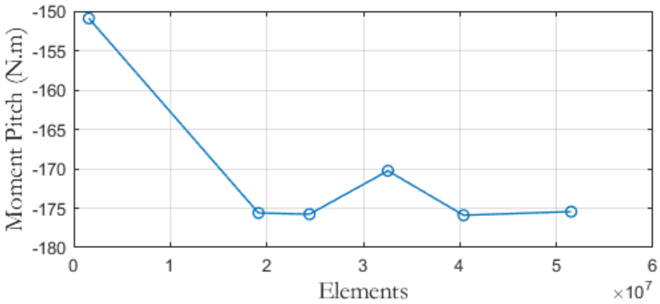

Fig. 4. Moment Pitch for aircraft wall body.

2.3. Model Geometry and Wind Tunnels

The following is the geometry of the 19-passenger aircraft in the wind tunnel test model.

Table 2. The geometry of the 19-passenger plane model [17].

Geometry		
Area	41.5	m2
Aspect Ratio	9.165	
Taper Ratio	0.515	
Twist Angle	0	deg
Sweepback at 1/4 chord	0	deg
Dihedral	0	deg
Root chord	2.81	m
SOB chord	2.67	m
Tip chord	1.447	m
Half span	9.75	m
SOB span	1	m
MAC	2.201	m
Aileron chord	30	%
Aileron type	plain	
Main Aerofoil chord	87	%
Flap chord	30	%
Flap Type	DSF	

The main test facility of UPT LAGG BPPT is a closed-circuit Low-Speed Wind Tunnel (Indonesian Low-Speed Tunnel) having a central tunnel section with a total length of 67.5 m, a width of 18 m, and a height of 5.5 m above the ground. The size of the cross-section of the test chamber (test section) is 4 m x 3 m, length of 10 m; see Fig. 5 [18]. LAGG is a professional wind tunnel used by the industry.

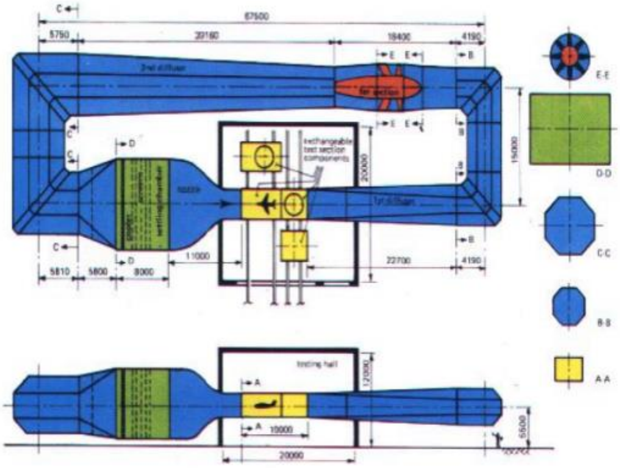

Fig. 5. ILST wind tunnel geometry [18], [19], [20].

2.4. Testing Process

The test parameters were carried out on a 19-passenger aircraft model at ILST by varying the angle of attack, horizontal tail angle, flap angle, HTP position, and speed set at 70 m/s. The testing process of this model is done by installing the model on the strut provided, namely the wing strut, where the model will be connected by two struts. An illustration can be seen in Fig. 6.

Fig. 6. Overview of the model setup in ILST [21], [22].

2.5. Data Processing

The calculation process carried out to obtain the downwash angle is to take the value of the Coefficient of Moment (C_M), data that has been processed for both tail-off and tail-on configurations.

Downwash is calculated using the equation [23], [24]

$$\varepsilon + \alpha_{0H} = \alpha_B - i_W + i_H - \frac{\Delta C_M}{C_{M_{iH}}} \tag{8}$$

Where to calculate the moment coefficient delta with variations in the angle of attack using the equation

$$\Delta C_M = C_{M_{TailOn}} - C_{M_{TailOff}} \Big|_{\alpha} \tag{9}$$

And calculate with variations in the angle of attack

$$C_{M_{iH}} = \left. \frac{C_{M_{iH1}} - C_{M_{iH2}}}{i_{H1} - i_{H2}} \right|_{\alpha} \tag{10}$$

equal :

$$\alpha_h = \alpha_B + i_h - \varepsilon \tag{11}$$

The angle of attack horizontal = angle of attack body + incidence horizontal – downwash.

The flow of data processing to obtain the downwash angle is as follows :

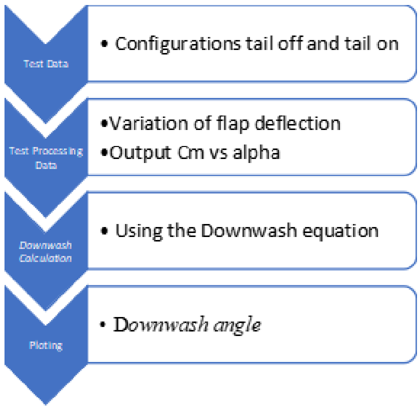

Fig. 7. Flow chart data processing of wind tunnel.

Several data corrections have been applied to wind tunnel test results, including:

- Weight correction
- Zero correction
- Tunnel wall disturbance correction
- Solid blockage correction
- Tare force correction

3. Research Results and Discussion

3.1. Simulation Results

The simulation is carried out by varying the different pairs of tail positions, which are symbolized as H61, H62, and H63. The results obtained are graphs of the lift force coefficient and pitch moment coefficient.

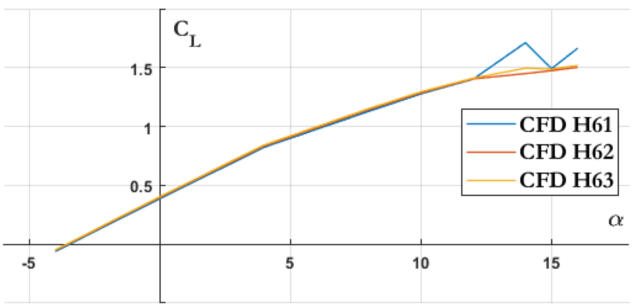

Fig. 8. CL vs Angle of Attack at flap=0.

Figure 8 shows the lift coefficient relative to the change in angle of attack at flap=0. From Fig. 8, it can be seen that the trend line is the same, and the different tide positions of H61, H62, and H63 do not have a significant effect.

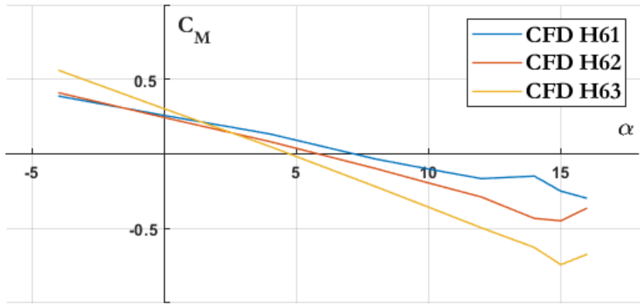

Fig. 9. C_M vs Angle of Attack at flap=0.

Figure 9 shows the pitch moment coefficient relative to the change in angle of attack at flap=0. From Fig. 9, the difference in the pitch moment character can be seen where the H61 tail configuration is smaller than the H62 and H63 tail configurations.

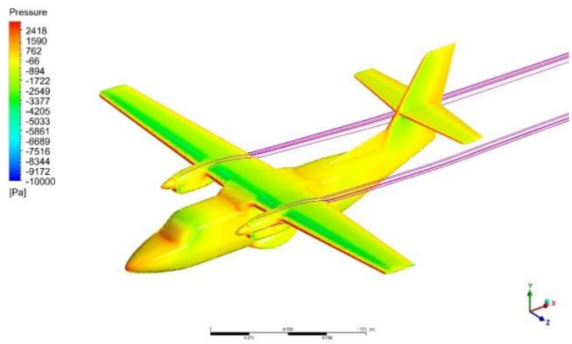

Fig. 10. Pressure distribution in aircraft and flow of downwash.

Figure 10 shows the pressure distribution on a 19-passenger aircraft and the downwash flow in the H61 tail configuration. The red color shows a greater pressure level, while the blue color shows a small pressure level. The greatest pressure is experienced on the front surface of the aircraft.

Figure 11 shows the pressure distribution at different tail tide positions. Pressure changes occur on the surface of each tile configuration. The greatest pressure occurs on the front surface of the tail (leading edge).

Figure 12 shows the flow visualization of the downwash flow for aircraft when the angle of attack changes with different tail positions. From Fig. 12, it can be seen that the downwash flow in the H61 tail configuration hit the tail at an angle of attack of 14°, while for H62 and H63, it hit at an angle of attack of 16°.

The downwash angle from the simulation results cannot be obtained with certainty, but some references can help calculate the downwash angle. In this investigation, the downwash angle was obtained from wind tunnel test results.

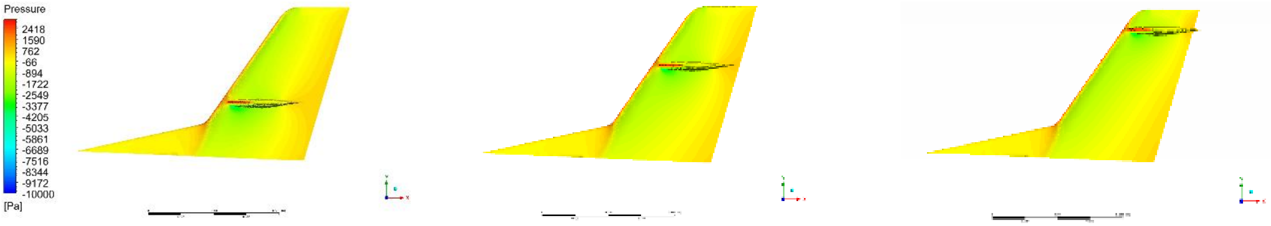

Fig. 11. Pressure distribution at the tail of H61, H62, H6.

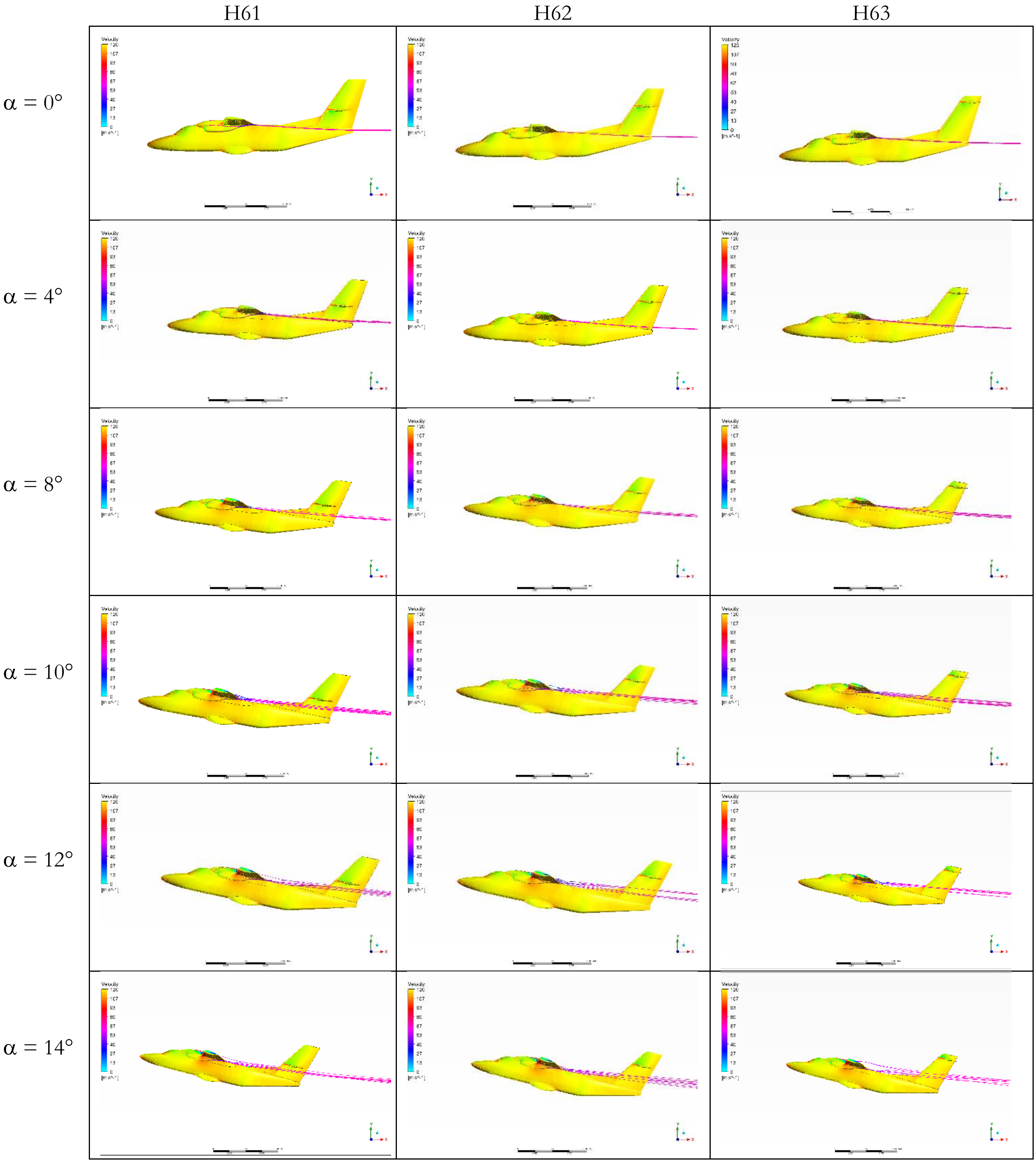

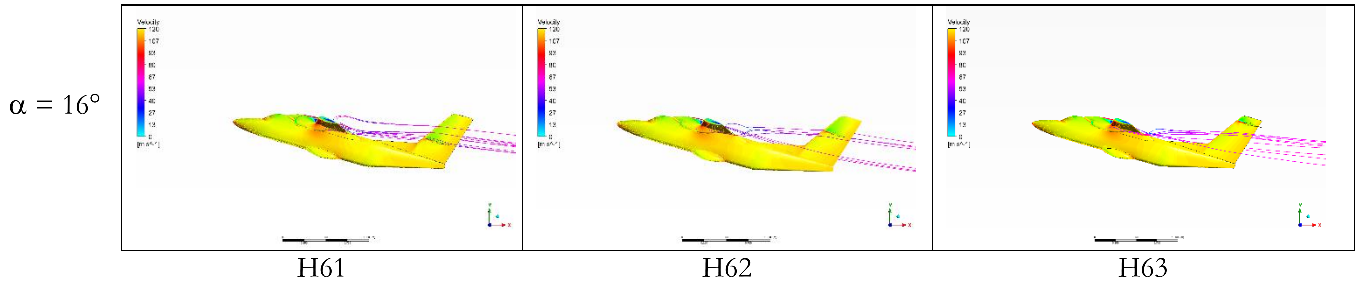

Fig. 12. Flow visualization of downwash flow at a variant of tail and angle of attack.

3.2. Wind Tunnel Results

From the processing of the wind tunnel test data, the data for all configurations tested will be analyzed to obtain the downwash angle and dynamic pressure on the horizontal tail [25]. In this case, we only calculate the downwash angle from the wind tunnel results.

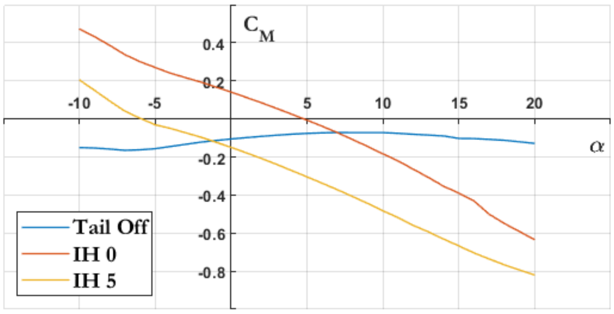

$C_{M\alpha}$ at Flap 0°

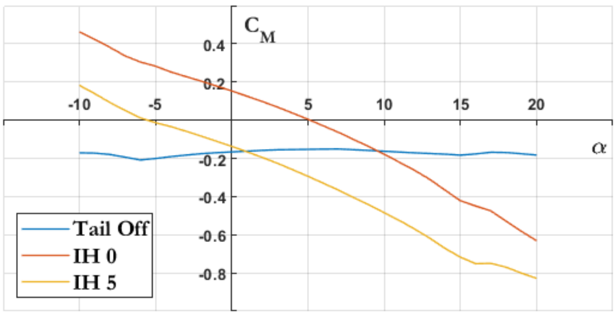

$C_{M\alpha}$ at Flap 10°

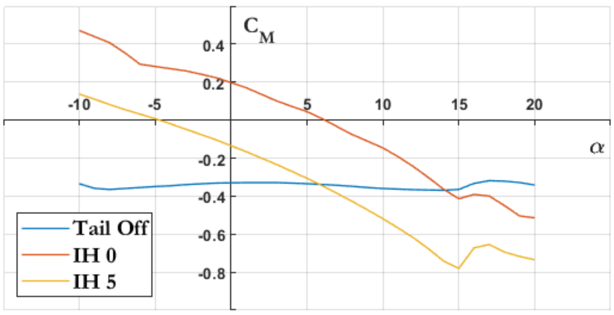

$C_{M\alpha}$ at Flap 40°

Fig. 13. Changes in C_M to Angle of Attack between tailless and tailless for the H61 configuration and changes in flap deflection.

The graph in Fig. 13 shows the C_M graph for the angle of attack with a different flap deflection for the H61 configuration. From this graph, what will be seen is the intersection of the C_M values between the configuration without a tail (tail off) and the configuration with a tail (H61), where for the HTP pairing angle 5° with flap deflection of 0° it can be seen that the point of intersection is at an angle of attack of -1°, while a flap of 10° is at an angle of attack of 1° and a deflection of 40° is at an angle of attack of 6°. For the HTP angle of 0° with 0° flap deflection, it can be seen that the point of intersection is at an angle of attack of 7°, while a 10° flap deflection is at an angle of attack of 9°, and a deflection of 40° is at an angle of attack of 14°.

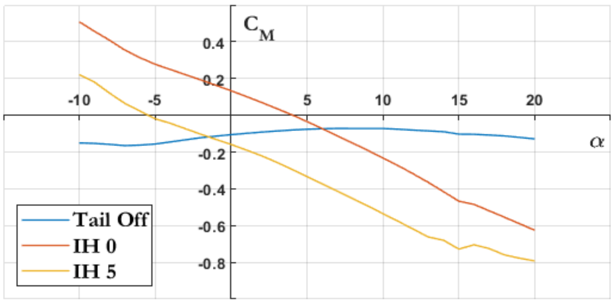

$C_{M\alpha}$ at Flap 0°

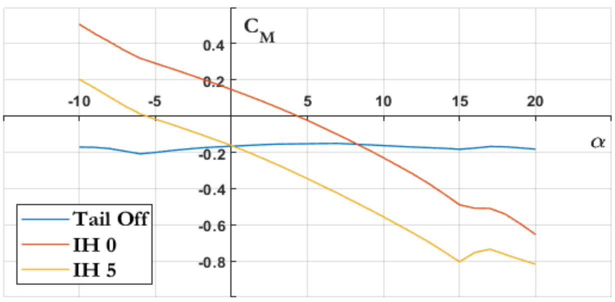

$C_{M\alpha}$ at Flap 10°

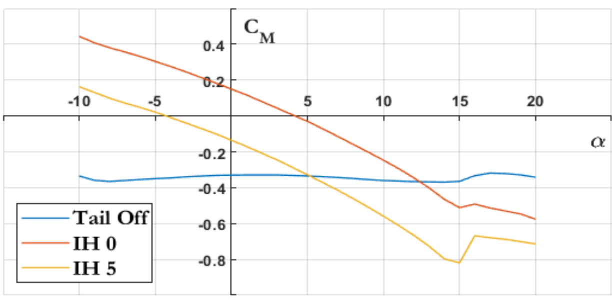

$C_{M\alpha}$ at Flap 40°

Fig. 14. Changes in C_M to Angle of Attack between tailless and tailless for the H62 configuration and changes in flap deflection.

The graph in Fig. 14 shows the C_M graph for the angle of attack with a different flap deflection for the H62 configuration. From this graph, what will be seen is the intersection of the C_M values between the configuration without a tail (tail off) and the configuration with a tail (H62), where for the HTP angle 5° with a 0° flap deflection, it can be seen that point of intersection is at an angle of attack of -2°, while a 10° flap deflection is at an angle of attack of 0° and a 40° deflection is at an angle of attack of 5°. For HTP angle of 0° with 0° flap deflection, it can be seen that the point of intersection is at an angle of attack of 6°, while a 10° flap deflection is at an angle of attack of 8°, and a deflection of 40° is at an angle of attack of 12°.

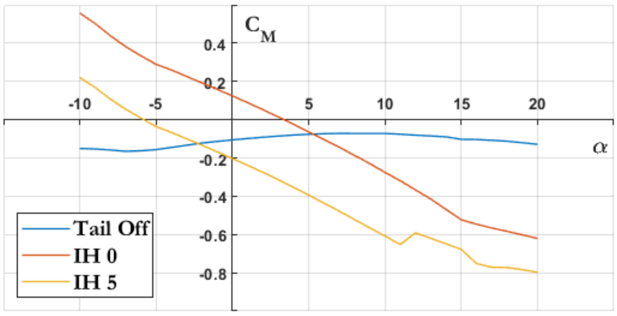

$C_{M\alpha}$ at Flap 0°

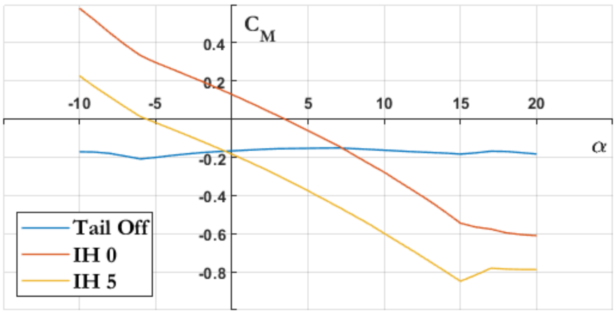

$C_{M\alpha}$ at Flap 10°

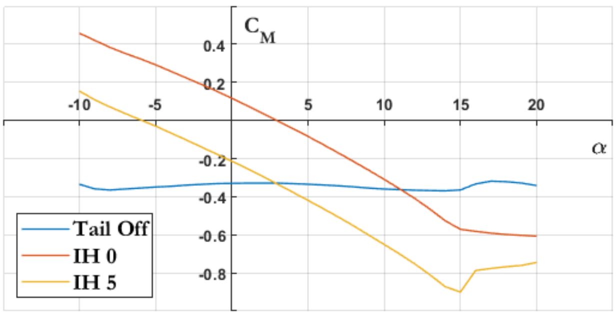

$C_{M\alpha}$ at Flap 40°

Fig. 15. Changes in C_M to Angle of Attack between tailless and tailless for the H63 configuration and changes in flap deflection.

Figure 15 shows the C_M graph for the angle of attack with different flap deflections for the H63 configuration. This graph is the result of plotting; what will be seen is the intersection of the C_M values between the configuration without a tail (tail off) and the configuration with a tail (H63), where the HTP mounting angle of 5° with a flap deflection of 0° it can be seen that the point of intersection is at an angle of attack -2°, while a 10° flap deflection is at an angle of attack of 0° and a 40° deflection is at an angle of attack of 3°. For an HTP angle of 0° with 0° flap deflection, it can be seen that the point of intersection is at an angle of attack of 5°, while a 10° flap deflection is at an angle of attack of 7°, and a deflection of 40° is at an angle of attack of 11°.

So, to prove this, calculations are carried out using the equation to calculate downwash. The initial step to obtaining the value of the downwash angle is to calculate the value of the moment coefficient delta with variations in the tidal angle and flap deflection. In this paper, different configuration positions of the horizontal tail are carried out with tidal angles of 0° and 5°.

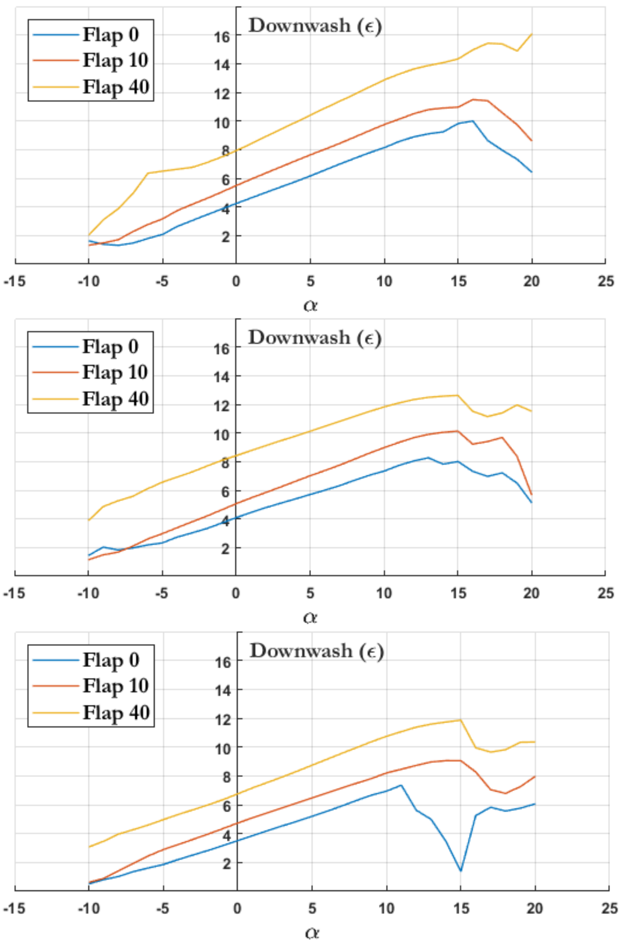

Fig. 16. Changes in downwash angle to changes in flap deflection for the H61, H62, and H63 configurations.

Figure 16 shows the change in downwash angle to the change in angle of attack for the H61, H62, and H63 configurations with different flap deflections. From the three images, it can be seen that as the flap deflection increases, the downwash angle also increases.

Figure 17 shows the change in the downwash angle to the change in the angle of attack for different flap deflections with the H61, H62, and H63 configurations. From the three images, it can be seen that as the flap deflection increases, the downwash angle also increases.

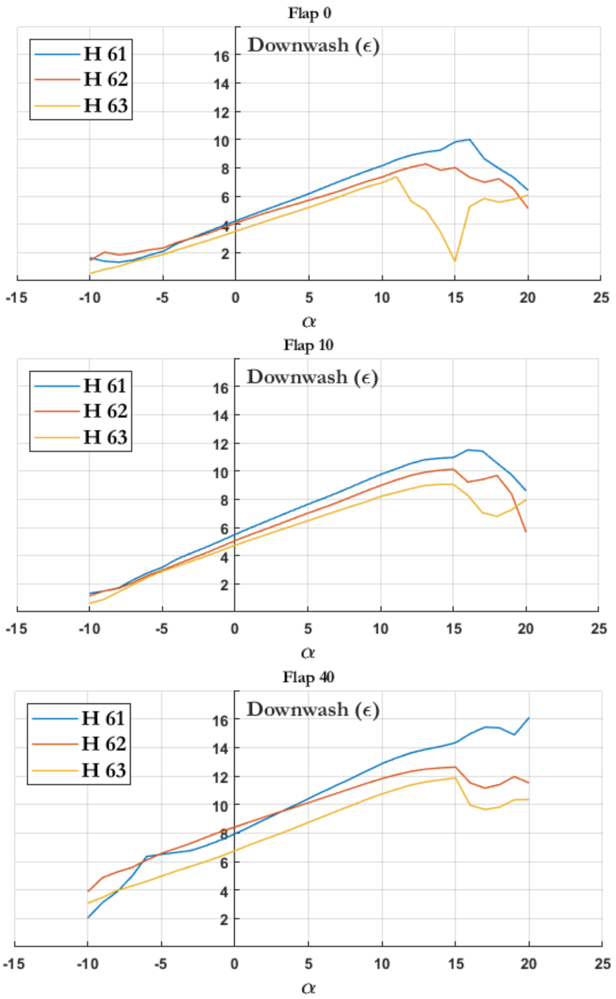

Fig. 17. Changes in downwash angle to HTP configuration changes at 0°, 10°, and 40°.

Table 3. Calculation results of downwash angle of attack and downwash angle at an angle of attack of 0° with changes in the flap angle.

Configuration	δε/δα	ε0
	Flap 0 deg	
H61	0.3850	4.25
H62	0.3861	4.09
H63	0.3455	3.51
	Flap 10 deg	
H61	0.4282	5.50
H62	0.4012	5.06
H63	0.3640	4.73
	Flap 40 deg	
H61	0.4541	7.94
H62	0.3494	8.41
H63	0.4114	6.76

3.3. Comparison Simulation and Wind Tunnel

To see the comparison between the simulation and the wind tunnel test results, look at the pitch moment, which is displayed in graphic form below (Fig. 18)

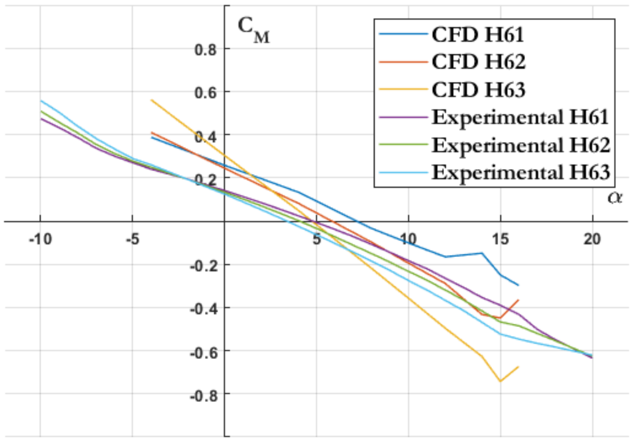

Fig. 18. Comparison between simulation and wind tunnel test at flap 0.

In Fig. 18, you can see the trend line of the pitch moment from simulation results and wind tunnel tests at flap 0. The results of the pitch moment coefficient are not very significant between the simulation and the wind tunnel results.

4. Conclusion

In the downwash investigation with wind tunnel testing, it can be concluded that :

1) The flap deflection greatly affects the downwash felt by the HTP. The greater the resulting flap downwash deflection, the greater the value of the downwash angle will change with the angle of attack.
2) Slope downwash and angle of attack when the angle of attack is 0°, $\delta\varepsilon/\delta\alpha = 0.386$ for the H62 configuration.
3) This downwash will later be used to see the contribution of HTP to the aircraft configuration.
4) The comparison between the simulation and the wind tunnel has the same trend at the pitch moment.

Acknowledgments

Thanks to LAPAN/BRIN and PT DI for facilitating this research and friends who supported this activity, especially Fadilah Hasim, head of the aviation technology research center, and Seszy Yunioritta, who guided the data processing.

Author Contributions

A not sole author manuscript must write their contribution statement. The contribution statement may be written in detail as follows (Note: the author's initials are DH, ARS, AA, AS, STP, and DT): DH developed the simulation and experiments data, designed the method, and prepared the manuscript, ARS, AA, and AS analyzed the results of simulation and prepared the manuscript, STP developed data processing of experiments results, and DT prepared the manuscript. The contribution statement may also be written as follows: DH, ARS, AA, AS, STP, and DT are the main contributor.

References

[1] M. Mahdi, "Prediction of wing downwash using CFD," *INCAS Bulletin*, vol. 7, no. 2, 2015. doi: 10.13111/2066-8201.2015.7.2.10.

[2] Wikipedia, "Downwash," [Online]. Available: https://en.wikipedia.org/wiki/Downwash. [Accessed: Jun. 8, 2022].

[3] G. Brebner, "The control of guided weapons," AGARD LS-85, 1976.

[4] A. R. Davari and M. R. Azimian, "Effects of wing geometry on wing-body-tail interference in subsonic flow," *Scientia Iranica B*, vol. 18, no. 3, pp. 407-415, 2011. doi: 10.1016/j.scient.2011.05.031.

[5] G. Wijiatmoko, "Analisa aerodinamika pengaruh landing gear pada pesawat udara nir awak (PUNA) alap-alap," in Proceedings of the National Seminar on Innovation and Technology Applications in Industry, Malang, Indonesia, 2017. doi: 10.36040/seniati.v3i2.2021.

[6] Y. Daryanto and J. P. Nugroho, "Wing configuration on wind tunnel testing of an unmanned aircraft vehicle," *Journal of Physics: Conference Series*, vol. 1005, no. 1, 2018. doi: 10.1088/1742-6596/1005/1/012032.

[7] S. Kayhan and S. Ozgen, "Sizing and optimization of the horizontal tail of a jet trainer," in Proceedings of the 8th European Conference for Aeronautics and Space Sciences (EUCASS), Madrid, Spain, 2019.

[8] D. Herdiana, "The effect of slipstream flow by propeller on wings of aerodynamic characteristics of UAV HALE aircraft," Master's thesis, Bandung Institute of Technology (ITB), Bandung, Indonesia, 2021.

[9] S. D. Launder and B. E. Spalding, "The numerical computation of turbulent flows," *Computer Methods in Applied Mechanics and Engineering*, vol. 3, no. 2, pp. 269–289, 1974. doi: 10.1016/0045-7825(74)90029-2.

[10] W. D. Cole, "Re-assessment of the scale-determining equation for advanced turbulence models," *AIAA Journal*, vol. 26, no. 11, pp. 1299–1310, 1988. doi: 10.2514/3.10041.

[11] F. Menter, "Review of the shear-stress transport turbulence model experience from an industrial perspective," *International Journal of Computational Fluid Dynamics*, vol. 23, no. 1–4, pp. 277–303, 2009. doi: 10.1080/10618560902773387.

[12] M. F. Rodi, "Zonal two-equation k- turbulence model for aerodynamic flows," *AIAA Journal*, no. 93-2906, 1993. doi: 10.2514/6.1993-2906.

[13] U. F. Gamiz, "Fluid dynamic characterization of vortex generators and two-dimensional turbulent wakes," Ph.D. dissertation, Polytechnic University of Catalonia (UPC), Spain, 2013.

[14] S. N. Sørensen, "General-purpose flow solver applied to flow over hills," Technical Report Risoe-R-827(EN), Risoe National Laboratory, 1995.

[15] A. Suprianto, F. Hartono, D. Herdiana, D. Tresnoningrum, and N. Pramana, "Pusher propeller performance investigation on lightweight medium-range UAV," *Engineering Journal*, vol. 28, no. 9, pp. 11–24, Sep. 2024. doi: 10.4186/ej.2024.28.9.11.

[16] ANSYS, Inc., *ANSYS Software Package, Version 23.0*, 2023.

[17] PT DI, "D519ND-006," Internal Document, 2014.

[18] PT DI, "Data WTT EXP 180," Internal Document, 2014.

[19] A. F. Iskandar, "Uji aerodinamika model kapal bersayap 'wing in surface effect' sebagai input kajian gerak planning menjelang take-off," Jurnal Teknologi Dirgantara, vol. 8, no. 1, pp. 1–11, 2010.

[20] UPT LAGG, "PUNA wind tunnel model scale 1:2.4 drawings," Internal Document, 2014.

[21] A. R. Soemaryanto, D. Herdiana, W. Wahyudi, R. Triwulandari, and M. N. Aziz, "Parametric study of extended horizontal tailplane of commuter aircraft using wind tunnel testing," in *AIP Conference Proceedings*, vol. 2941, no. 1, Dec. 2023. doi: 10.1063/5.0181442.

[22] PT DI, "D519ND-003," Internal Document, 2014.

[23] PT DI, "D510ND-006," Internal Document, 2014.

[24] S. Karatoprak, "Sizing and optimization of the horizontal tail of a jet trainer," M.Sc. thesis, Middle East Technical University, Turkey, 2019.

[25] PT DI, "Stability and control analysis," Internal Presentation Slides, 2014.

Dana Herdiana was born in Bandung, West Java, Indonesia in 1980. He received the S.T. degree in aerospace engineering from the Nurtanio University, Bandung, in 2004 and the M.T. degree in aerospace engineering from Bandung Institute of Technology, Bandung, in 2021.

From 2006 to 2021, he worked at LAPAN, and the institution changed to BRIN. From 2021 to now, he has worked at BRIN. The research he does in his work is in the field of aerodynamics. Articles related to aerodynamics have been published in several journals and proceedings. His research interests include aerodynamics simulation or experiments, the design of parachutes, downwash, slipstream, and aircraft performance. Dana Herdiana, ST., MT., was a member of The Indonesian Research Association (PPI).

Sinung Tirtha Pinindriya holds a Bachelor of Engineering (B.Eng.) degree in Mechanical Engineering from Universitas Muhammadiyah Surakarta in 2005, and he also holds a Master of Engineering (M.Eng.) degree in Mechanical Engineering from Universitas Gadjah Mada in 2017, besides having several professional certificates and skills. His research interests and experiences are in wind tunnel testing and towing tank testing for seaplanes and performing CFD simulations for his research.

Arifin Rasyadi Soemaryanto holds a Bachelor of Engineering degree in Aeronautics and Astronautics from Bandung Institute of Technology, Indonesia in 2011. Currently, he is a researcher at the Research Center of Aeronautics Technology, National Research and Innovation Agency (BRIN), Indonesia. He has experience in the aerodynamic design of aerial vehicles and some of the subject multi-disciplines, such as hydrodynamics. At the moment, his research interests are in the design optimization of aerial vehicles.

Agus Aribowo completed a bachelor's degree in 1994 and a master's degree in 1999 in mechanical engineering at Okayama University, Japan. He was interested in research in the field of Aerodynamics, both numerical and experimental simulations. He was involved in several aircraft development programs, such as the N219 aircraft and also the N219 Amphibious aircraft.

Agus Suprianto was born in Jakarta, Indonesia, in 1986. In 2010, he received a Bachelor's degree in aeronautical engineering with a concentration in propulsion from Air Marshal Suryadarma University, East Jakarta. In 2019, he received a Master's degree in aerospace engineering with a concentration in aerodynamic propulsion from Bandung Institute of Technology, Bandung.

He worked at BPPT from 2011 to 2021, and the institution later changed to BRIN. He has been working at BRIN since 2021. He conducts research in the fields of aerodynamics, propulsion design, and the performance of UAVs. His research interests include aerodynamics and propulsion simulation or experiments, the design of high-altitude propellers, the programming of aircraft performance, and the conceptual design of electric aircraft.

Deasy Tresnoningrum was born in Jakarta, Indonesia, in 1984. In 2007, she received a Bachelor's degree in astronomy, and in 2020, she obtained a Master's degree in aerospace engineering with a concentration in flight mechanics. These degrees were earned from the Bandung Institute of Technology (ITB) in Bandung, Indonesia.

She worked at LAPAN from 2008 to 2021, and the institution has since changed its name to BRIN. She has been working at BRIN since 2021. Her research work is focused on the flight dynamics of aircraft. Her research interests include aircraft performance, aircraft flight dynamics simulation and analysis, and aircraft conceptual design.